

Direct observation of myoglobin structural dynamics from 100 picoseconds to 1 microsecond with picosecond X-ray solution scattering†‡

Kyung Hwan Kim, Key Young Oang, Jeongho Kim, Jae Hyuk Lee, Youngmin Kim and Hyotcherl Ihee*

Received 10th June 2010, Accepted 26th July 2010

DOI: 10.1039/c0cc01817a

Here we report structural dynamics of equine myoglobin (Mb) in response to the CO photodissociation visualized by picosecond time-resolved X-ray solution scattering. The data clearly reveal new structural dynamics that occur in the timescale of ~360 picoseconds (ps) and ~9 nanoseconds (ns), which have not been clearly detected in previous studies.

Myoglobin (Mb) is a heme protein that carries small-molecule ligands such as O₂, CO and NO in muscles, and can be considered as a subunit of hemoglobin, a paradigm protein for the study of allostery. Due to its small size, availability and photosensitivity of the heme–ligand bond, Mb has served as a prototypical model system for studying protein structural dynamics. Accordingly, structural dynamics of Mb have been intensively studied with various spectroscopic^{1–8} and structural^{9–16} tools. The ligands form covalent bonds with Fe²⁺ of the heme group and can be photolyzed by visible light on the sub-picosecond timescale.^{2,3} Upon the CO photolysis of MbCO, a small portion of the dissociated CO ligands geminately rebind to the heme, while the remainder travel to various pockets that can accommodate the ligand and eventually escape the protein matrix to the solvent. On a longer timescale, the vacant heme recovers the ligand *via* non-geminate recombination.

To directly track the structural changes associated with the ligand migration and rebinding and capture structurally distinct intermediates, we used the pump-probe time-resolved X-ray solution scattering technique, where the time-dependent scattering of short X-ray pulses from a synchrotron are used to interrogate the structural dynamics of a liquid solution sample that is pumped with optical laser pulses in a pump-probe manner. Time-resolved X-ray solution scattering^{17–19} together with time-resolved X-ray crystallography,²⁰ X-ray absorption spectroscopy²¹ and electron diffraction²¹ can provide direct structural information, and thus complements time-resolved optical spectroscopy in the analysis of solution-phase reaction mechanisms. Recently the time-resolved solution scattering technique has been applied to follow conformational changes in proteins with nanosecond^{22–24} and picosecond²⁵ time resolution.

Here, we show its application to another type of protein, Mb from equine heart, with picosecond time resolution.

Time-resolved X-ray solution scattering data were measured at 14IDB beamline of Advanced Photon Source. The usual experimental protocol^{22,25} was followed. Specifically, equine heart MbCO solution (8 mM, pH 7.0, 0.1 M sodium phosphate) filled in a quartz capillary was excited by a ~30 ps-long laser pulse at 532 nm to initiate the CO photodissociation, and a ~100-ps-long single X-ray pulse was sent to the sample at a well-defined time delay with respect to the arrival of the laser pulse. The scattered X-rays were recorded in a CCD detector as a function of the time delay between the laser and X-ray pulses. Fig. 1A shows the difference X-ray scattering data measured for a wide time range spanning from 100 ps to 1 μ s. The difference scattering curves, $\Delta S(q, t)$, were obtained by subtracting the scattering curve measured at -5μ s from the curves at various (positive) time delays, *i.e.*, $\Delta S(q, t) = S(q, t) - S(q, -5 \mu$ s). Oscillatory features are clear in the difference curves at all time delays. Most of the features in the difference signal develop within 100 ps, but some features still evolve afterwards. To magnify the subtle changes, double difference curves ($\Delta\Delta S(q, t; t_{\text{ref}}) = \Delta S(q, t) - \Delta S(q, t_{\text{ref}})$) were obtained between the difference curves at two different time delays using various reference time points (100 ps, 1 ns, 10 ns and 70 ns). For example, $\Delta\Delta S(q, t; 100 \text{ ps})$ highlights the change occurring between t and 100 ps time delays. Close inspection of the time-resolved X-ray scattering data reveals four distinct transitions well separated in timescales. The first one occurs at 300–500 ps, the second at 1–10 ns, the third at 10–100 ns, the fourth at 100 ns–1 μ s. Difference curves at representative time delays for each time region are compared in Fig. 1C.

The data at 0 ps and 100 ps are identical within our experimental error if the data at 0 ps is doubled (as shown in Fig. 1A) to compensate for the delayed signal buildup due to half overlap between the pump and probe pulses at 0 ps. The agreement between the two data indicates that a significant degree of tertiary structural changes occurs faster than the time resolution of our experiment, resulting in the 0 ps signal with the same oscillatory features as in the 100 ps signal. As time goes on, the negative peak around $q = 0.7 \text{ \AA}^{-1}$ (p3 region) grows in two steps on the timescales of 300–500 ps and 1–10 ns. The negative peak around $q = 0.35 \text{ \AA}^{-1}$ (p2 region) increases (*i.e.*, becomes more negative) on the 1–10 ns timescale and then decreases (*i.e.*, becomes less negative) in 10–100 ns. These changes can be more clearly seen in the double difference curves. For example, $\Delta\Delta S(q, 10 \text{ ns}; 1 \text{ ns})$ is negative whereas $\Delta\Delta S(q, 100 \text{ ns}; 10 \text{ ns})$ is positive around $q = 0.35 \text{ \AA}^{-1}$. On the

Center for Time-Resolved Diffraction, Department of Chemistry, Graduate School of Nanoscience & Technology (WCU), KAIST, Daejeon 305-701, Korea. E-mail: hyotcherl.ihee@kaist.ac.kr; Fax: (+82) 42-350-2810; Tel: (+82) 42-350-2884

† This article is part of the 'Emerging Investigators' themed issue for ChemComm.

‡ Electronic supplementary information (ESI) available: Data collection protocol, data processing and data analysis. See DOI: 10.1039/c0cc01817a

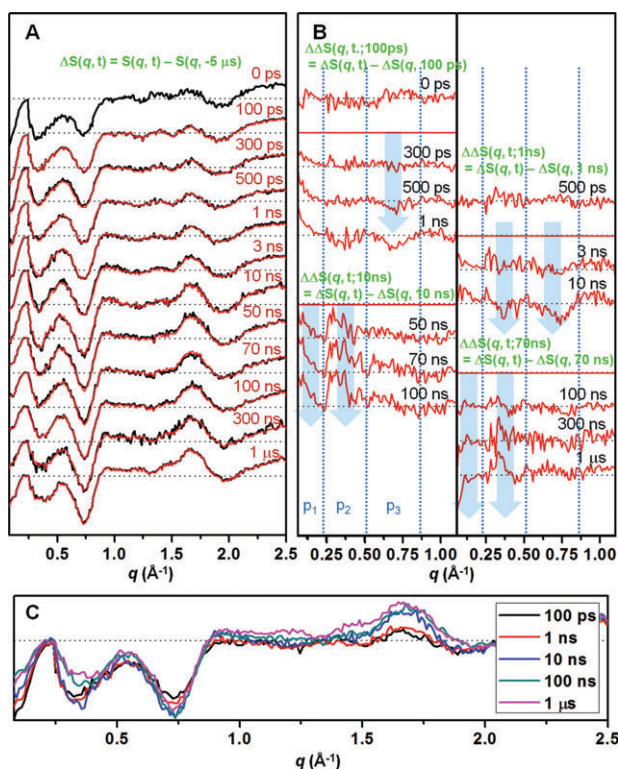


Fig. 1 (A) Time-resolved X-ray solution scattering data for MbCO \rightarrow Mb + CO in solution at representative time delays from 0 ps to 1 μ s. The black curves are experimental difference curves ($\Delta S(q, t) = S(q, t) - S(q, -5 \mu\text{s})$) obtained by subtracting the scattering curve at $-5 \mu\text{s}$ from the curves at other time delays. The red curves are theoretical data obtained from principal component analysis. Here the theoretical data is a linear sum of species-associated scattering curves obeying a simple sequential kinetic model. For the sake of presentation, the signals below $q = 0.22 \text{ \AA}^{-1}$ were divided by 6. (B) To emphasize subtle changes at the low angle ($q = 0.07\text{--}1.1 \text{ \AA}^{-1}$), double difference curves ($\Delta\Delta S(q, t; t_{\text{ref}}) = \Delta S(q, t) - \Delta S(q, t_{\text{ref}})$) obtained with various reference time points (100 ps, 1 ns, 10 ns and 70 ns). Each curve was scaled by a factor of 2 to magnify small changes. Transitions in 300–500 ps, 1–10 ns, 10–100 ns and 100 ns–1 μ s time ranges are clearly identified. Blue arrows are shown to guide q positions where major changes occur. In (A) and (B), the data corresponding to a common time delay are shown aligned at the same vertical position. (C) Difference curves at representative time delays are shown in higher magnification than in (A).

timescale of 10–100 ns, the negative signal at low q (p1 region) decreases (*i.e.*, becomes less negative) and thus $\Delta\Delta S(q, t; 10 \text{ ns})$ becomes more positive on this timescale. In 100 ns–1 μ s, the peak around $q = 0.35 \text{ \AA}^{-1}$ broadens and the negative signal at low q (p1 region) increases (*i.e.*, becomes more negative).

Quantitative analysis was also conducted by using singular value decomposition (SVD) and principal component analysis. We first applied singular value decomposition to the data. The first four principal time-dependent components (right singular vectors) can be simultaneously fitted with four exponentials of distinct time constants; 360 ps, 9 ns, 70 ns and 150 ns (Fig. 2A). We note that these time constants are consistent with the qualitative estimations outlined in Fig. 1. Using these time constants, we then applied principal component analysis using a simple sequential kinetic mechanism. From

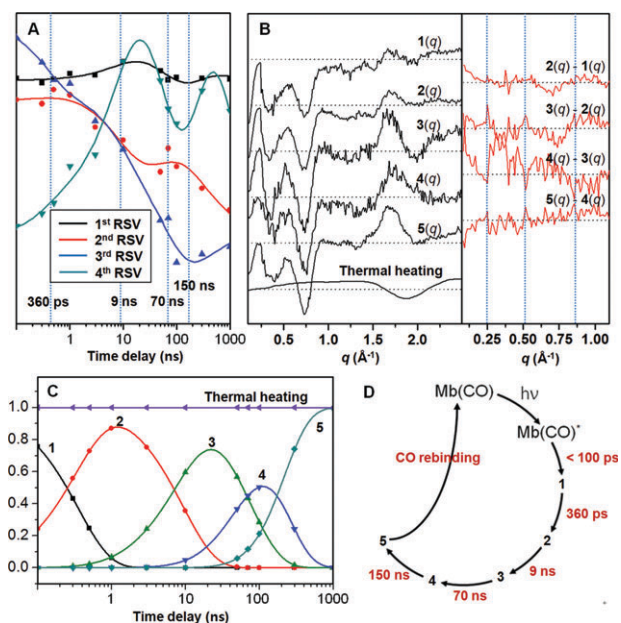


Fig. 2 (A) The first four principal time-dependent components from SVD analysis can be simultaneously fitted with a sum of four exponentials, yielding the following time constants: 360 ps, 9 ns, 70 ns, 150 ns. (B) (Left) Five species-associated difference scattering curves can be extracted *via* principal component analysis where the time constants from the SVD analysis were used. (Right) The double difference curves between temporally adjacent species are also shown in the same manner as in Fig. 1B, in order to bring out subtle changes at the low angle. (C) Population changes of reaction intermediates. (D) Reaction kinetics of MbCO photolysis.

the analysis, by minimizing the discrepancy between theory and experiment, species-associated difference scattering curves corresponding to five intermediates (1 to 5) were extracted as shown in Fig. 2B. These species-associated scattering curves obey a sequential kinetic model with the time constants extracted from the SVD analysis and theoretical scattering curves at various time delays are well represented by a linear combination of those species-associated scattering curves as shown in Fig. 1. One caveat is that this does not necessarily mean the sequential kinetic model is the best one. The population changes of the reaction intermediates are shown in Fig. 2C and the photocycle of MbCO is summarized in Fig. 2D.

The intermediates identified with distinct time constants from our analysis actually represent *structurally distinct* intermediates that are uniquely detected by X-ray scattering and thus give us information complementary to optical spectroscopy. Structural analysis of the species-associated scattering curves will reveal detailed structural transitions such as time-dependent helix movements, and work is in progress in this regard.²³ Here we simply compare the four time constants with those obtained from optical spectroscopy. The late two time-scales ($\tau_{3 \rightarrow 4} = 70 \text{ ns}$ and $\tau_{4 \rightarrow 5} = 150 \text{ ns}$) determined from our TR-WAXS study can be interpreted in the framework of the most well accepted four-state model¹ ($A \rightarrow B \rightarrow C \rightarrow D \rightarrow S$), where A means the MbCO, B is the Mb with CO still in the heme pocket, C and D are the intermediate states where the CO is located in some pockets and S means the Mb with free

CO (in other words CO has completely escaped to the solvent). It is well established that B is populated on an ultrafast timescale within 10 ps ($\tau_{AB} < 10$ ps),²⁶ much shorter than our TR-WAXS time resolution. Various spectroscopic measurements established $\tau_{CD} \sim 70$ ns⁴ and $\tau_{DS} \sim 700$ ns.^{4,27} In particular, the $\tau_{3 \rightarrow 4}$ transition coincides with the $\tau_{CD} \sim 70$ ns decay component of the heterodyne-detected transient grating signal,⁴ which was assigned to transit time for ligand migration within Mb. Also, $\tau_{4 \rightarrow 5} = 150$ ns transition is on the same order of magnitude with the $\tau_{DS} \sim 700$ ns decay component in the transient grating signal.^{4,7} This component was assigned to the escape of the photodissociated CO from the protein matrix to the solvent based on the fact that the escape of the CO ligand from the protein matrix induces a considerable volume change. It can be seen from Fig. 1 and 2B that the negative signal at low q values, which is known to be sensitive to the electron density of the protein, increases (*i.e.*, becomes more negative) and this is consistent with the CO escape process. A very similar time constant (~ 180 ns) assigned to geminate rebinding of the CO molecule was observed from transient absorption spectroscopy,²⁸ but our 170 ns process should be related with CO escape since the decreased scattering intensity at the low q region cannot be explained by the geminate recombination process alone.

The early two transitions ($\tau_{1 \rightarrow 2} = 360$ ps and $\tau_{2 \rightarrow 3} = 9$ ns) observed in this study have been articulated to a much lesser extent relative to the late two transitions ($\tau_{3 \rightarrow 4}$ and $\tau_{4 \rightarrow 5}$). The closest to $\tau_{1 \rightarrow 2}$ is the ~ 300 ps decay component of the transient circular dichroism signal of the N band, which was assigned to conformational changes.⁶ However the later systematic CD study corrected this timescale to less than 100 ps.²⁹ It seems that there has been no direct observation of the B \rightarrow C process in the framework of the four-state model. According to some indirect estimation, τ_{BC} is about 180 ps.¹ This timescale is close to the $\tau_{1 \rightarrow 2} = 360$ ps timescale recovered from our data, but whether the $\tau_{1 \rightarrow 2}$ component can be assigned to the B \rightarrow C process is not certain because this B \rightarrow C process originally refers to the migration of CO rather than the structural transition of the protein matrix itself. The closest similarity to the $\tau_{2 \rightarrow 3} = 9$ ns transition is found in the time-resolved ultraviolet resonance Raman signal measured on the tryptophan and tyrosine Raman bands.⁵ In that work, it was suggested that the decay component on the 1–2.5 ns timescale can be attributed to the motion of the A helix toward the displaced E helix.

Recently, CO migration kinetics in a different type of Mb (from sperm whale) was studied using the same technique,²⁵ and the kinetics consisting of the exponentials of 74 ps, 2.7 ns, 220 ns and 5.7 μ s time constants were reported. Surprisingly, the kinetics and the shape of the scattering patterns of equine heart Mb and sperm whale Mb turn out to be very different. The origin of the difference in structural dynamics between the two Mb systems will be further investigated.

We acknowledge BioCARS staff for discussions and experimental assistance. This work was supported by the Creative Research Initiatives (Center for Time-Resolved Diffraction) of MEST/NRF. Use of the BioCARS Sector 14 was supported by NIH (RR007707). Time-resolved set-up at Sector 14 was

funded in part through a collaboration with Philip Anfinrud (NIH/NIDDK). We acknowledge the support from the WCU program.

Notes and references

- 1 D. Beece, L. Eisenstein, H. Frauenfelder, D. Good, M. C. Marden, L. Reinisch, A. H. Reynolds, L. B. Sorensen and K. T. Yue, *Biochemistry*, 1980, **19**, 5147–5157.
- 2 S. Franzen, B. Bohn, C. Poyart and J. L. Martin, *Biochemistry*, 1995, **34**, 1224–1237.
- 3 L. Richard, L. Genberg, J. Deak, H.-L. Chiu and R. J. D. Miller, *Biochemistry*, 1992, **31**, 10703–10715.
- 4 G. Dadusc, J. P. Ogilvie, P. Schulenberg, U. Marvet and R. J. D. Miller, *Proc. Natl. Acad. Sci. U. S. A.*, 2001, **98**, 6110–6115.
- 5 A. Sato and Y. Mizutani, *Biochemistry*, 2005, **44**, 14709–14714.
- 6 X. Xie and J. D. Simon, *Biochemistry*, 1991, **30**, 3682–3692.
- 7 M. Sakakura, S. Yamaguchi, N. Hitota and M. Terazima, *J. Am. Chem. Soc.*, 2001, **123**, 4286–4296.
- 8 L. Y. Zhang, L. J. Wang, Y. T. Kao, W. H. Qiu, Y. Yang, O. Okobiah and D. Zhong, *Proc. Natl. Acad. Sci. U. S. A.*, 2007, **104**, 18461–18466.
- 9 M. Schmidt, K. Nienhaus, R. Pahl, A. Krasselt, S. Anderson, F. Parak, G. U. Nienhaus and V. Srajer, *Proc. Natl. Acad. Sci. U. S. A.*, 2005, **102**, 11704–11709.
- 10 D. Bourgeois, B. Vallone, F. Schotte, A. Arcovito, A. E. Miele, G. Sciarra, M. Wulff, P. Anfinrud and M. Brunori, *Proc. Natl. Acad. Sci. U. S. A.*, 2003, **100**, 8704–8709.
- 11 A. Ostermann, R. Waschipky, F. G. Parak and G. U. Nienhaus, *Nature*, 2000, **404**, 205–208.
- 12 V. Srajer, T. Teng, T. Ursby, C. Pradervand, Z. Ren, S. Adachi, W. Schildkamp, D. Bourgeois, M. Wulff and K. Moffat, *Science*, 1996, **274**, 1726–1729.
- 13 F. Schotte, M. Lim, T. A. Jackson, A. V. Smirnov, J. Soman, J. S. Olson, G. N. J. Phillips, M. Wulff and P. Anfinrud, *Science*, 2003, **300**, 1944–1947.
- 14 M. L. Quillin, T. Li, J. S. Olson, G. N. Phillips Jr., Y. Dou, M. Ikeda-Saito, R. Regan, M. Carlson and Q. H. L. Gibson H., *J. Mol. Biol.*, 1995, **245**, 416–436.
- 15 R. Aranda, E. J. Levin, F. Schotte, P. A. Anfinrud and G. N. Phillips, *Acta Crystallogr., Sect. D: Biol. Crystallogr.*, 2006, **62**, 776–783.
- 16 K. Chu, J. Vojtechovsky, B. H. McMahon, R. M. Sweet, J. Berendzen and I. Schlichting, *Nature*, 2000, **403**, 921–923.
- 17 T. Ejdrup, H. T. Lemke, K. Haldrup, T. N. Nielsen, D. A. Arms, D. A. Walko, A. Miceli, E. C. Landahl, E. M. Dufresne and M. M. Nielsen, *J. Synchrotron Radiat.*, 2009, **16**, 387–390.
- 18 H. Ihee, *Acc. Chem. Res.*, 2009, **42**, 356–366.
- 19 J. Vincent, M. Andersson, M. Eklund, A. B. Wohri, M. Odelius, E. Malmerberg, Q. Y. Kong, M. Wulff, R. Neutze and J. Davidsson, *J. Chem. Phys.*, 2009, **130**.
- 20 K. Moffat, *Chem. Rev.*, 2001, **101**, 1569–1581.
- 21 M. Chergui and A. H. Zewail, *ChemPhysChem*, 2009, **10**, 28–43.
- 22 M. Cammarata, M. Levantino, F. Schotte, P. A. Anfinrud, F. Ewald, J. Choi, A. Cupane, M. Wulff and H. Ihee, *Nat. Methods*, 2008, **5**, 881–886.
- 23 S. Ahn, K. H. Kim, Y. Kim, J. Kim and H. Ihee, *J. Phys. Chem. B*, 2009, **113**, 13131–13133.
- 24 M. Andersson, E. Malmerberg, S. Westenhoff, G. Katona, M. Cammarata, A. B. Wohri, L. C. Johansson, F. Ewald, M. Eklund, M. Wulff, J. Davidsson and R. Neutze, *Structure*, 2009, **17**, 1265–1275.
- 25 H. S. Cho, N. Dashdorj, F. Schotte, T. Graber, R. Henning and P. Anfinrud, *Proc. Natl. Acad. Sci. U. S. A.*, 2010, **107**, 7281–7286.
- 26 L. Richard, L. Genberg, J. Deak, H.-L. Chiu and R. J. D. Miller, *Biochemistry*, 1992, **31**, 10703–10715.
- 27 M. Sakakura, S. Yamaguchi, N. Hirota and M. Terazima, *J. Am. Chem. Soc.*, 2001, **123**, 4286–4294.
- 28 E. R. Henry, J. H. Sommer, J. Hofrichter and W. A. Eaton, *J. Mol. Biol.*, 1983, **166**, 443–451.
- 29 T. Dartigalongue, C. Niezborala and F. Hache, *Phys. Chem. Chem. Phys.*, 2007, **9**, 1611–1615.